Materials Physics and Mechanics 47 (2021) 706-719
Research article

Received: May 21, 2020
Accepted: October 22, 2021

FINITE ELEMENT OF ROTATING WHEELSET AND ITS NATURAL FREQUENCIES DETERMINATION

Olimjon Ahmedov✉, Mirziyod Mirsaidov

Tashkent Institute of Irrigation and Agricultural Mechanization Engineers,

39, Kori Niyoziy St., Tashkent, Uzbekistan, 100000

✉ olimjon84@mail.ru

Abstract. This article is devoted to solving urgent problems related to the development of a mathematical model and methods for assessing the dynamic characteristics of railway wheelsets. In the simulation, railroad wheelsets are considered as a one-dimensional deformable body based on the Bernoulli-Euler theory with two rigid disks. The cross-section of the shaft is assumed flat and perpendicular to the centerline during vibration. Disks are modeled as a rigid body characterized by mass and moment of inertia. The centrifugal and gyroscopic effects and the damping properties of the material are taken into account. With these factors, the problem under consideration is reduced to a higher order of a homogeneous system of differential equations, which is then solved using the Altair Hyperworks and Matlab software. The dynamic characteristics of railway wheelsets are investigated depending on the angular speed of the wheel (without taking into account the contact between the wheelset and the rail), with and without damping. At that, a number of new mechanical effects were established.

Keywords: railway wheelsets, dynamic characteristics, eigenfrequencies and modes, damping, centrifugal and gyroscopic effects

***Acknowledgments**. No external funding was received for this study.*

Citation: Ahmedov Olimjon, Mirsaidov Mirziyod. Finite element of rotating wheelset and its natural frequencies determination // Materials Physics and Mechanics. 2021, V. 47. N. 5. P. 706-719. DOI: 10.18149/MPM.4752021_5.

1. Introduction

The study of the dynamic processes of various systems begins with the determination of dynamic characteristics, i.e., the determination of eigenfrequencies and corresponding vibration modes of the system. One of the main dynamic indices of rotating systems is the determination of eigenfrequencies and modes of vibration of the systems under consideration. The dynamic characteristics include eigenfrequencies, modes, and decrements of the system oscillations. Generally, dynamic characteristics are a passport of the system, which allows one to preliminarily estimate the dynamic properties of the system. Until recently, the determination of the dynamic characteristics of complex systems created a number of difficulties.

In recent years, significant advances in numerical modeling and computation of eigenfrequencies and modes of wave vibrations have greatly simplified design in all spheres

http://dx.doi.org/10.18149/MPM.4752021_5

of industry. However, at present time, the determination of dynamic characteristics and the prediction of dynamic properties of various systems are still complicated tasks and issues.

As is well known, the dynamic characteristics depend on the physical and geometric parameters of the system and determine the pattern of structural vibrations under various operating loads. Any strain in a linear structural system can be expressed as a linear combination of structural forms that set up an orthonormal vector base.

The results of dynamic analysis of the system are used in a variety of numerical simulation applications, including vibration sensitivity calculations, root cause analysis of induced vibrations, damage detection; they are used to provide flexibility in the analysis of a system of various bodies, to speed up calculations of durability and vibroacoustic properties. The results of evaluating these parameters of the system make it possible to efficiently calculate changes in the structure response to various impacts.

Classical monographs [1-4] describe the modeling of rotors, considering the disks as rigid bodies with their mass and moments of inertia.

In [5], the latest advances in the dynamic characteristics of the curve matching between the wheel and the rail were discussed. For modern railways, a framework and methodology were proposed that correspond to the characteristics of the dynamic interaction of a wheel and a rail on a curved track.

In [6], the setting up of a model was considered, intended to simulate the prediction of maximum dynamic torsional stresses to check the stability of railway wheelsets. That model assumed that vibration excitation comes from the wheel-rail contact point and that the vibration energy comes from the high-frequency drive control.

The study in [7] investigated the dynamic response of a wheel and a rail in the process of rolling contact for high-speed trains using the finite element method. The influence of the train speed on the wheel-rail contact forces was considered. The simulation results showed that the lateral and longitudinal wheel-rail contact forces are less than the corresponding vertical contact forces, and they appear to be insensitive to train speed.

In [8], two modeling methods were presented to analyze the dynamics of flexible wheelsets. The kinematics of the wheel profile is described taking into account the flexible displacements of the wheelset units. The Lagrange approach was used in modeling, to obtain all the terms of the equation of motion, including the inertial forces, and the Euler approach was used at the stage of integrating the equation of motion. A non-rotating finite element mesh of a wheelset was considered using the interpolation of flexible displacements at the nodes.

In [9], the model of flexible shafts was adapted to simulate a railroad wheelset. The dynamic properties of a rigid body were obtained from a rigid-body finite element model of a real wheelset. The model used the Euler axes set for numerical calculations. The results show that the gyroscopic effect can contribute to the determination of the wavelength fixing mechanism in some corrugation problems, even if the train speed is low.

In [10], the vertical dynamic interaction of a train and a track at high speeds of vehicle motion was investigated. The inertial effects caused by the rotation of the wheels were taken into account in the vehicle model by implementing the model of structural dynamics of the rotating wheelset. To test the model of train-to-rail interaction, the calculated contact forces were compared with the contact forces measured with an instrumental wheelset. It was stated that when the system was excited at a frequency at which two different wheelset modes (due to wheel rotation) have the same resonant frequencies, significant differences were found in the contact forces calculated using the models of rotating and non-rotating wheelset.

In [11], an analysis and comparison of the Hopf bifurcation behavior of a two-axle railway bogie and a double wheelset in the presence of nonlinearities in the form of damping forces in the longitudinal suspension system and a heuristic model of the creep of the wheel-

rail contact, including the gap clearance in the dead surface, when moving along a curved track were presented. Frequency power spectra at critical speeds, in subcritical and supercritical bifurcations, were presented by comparing a two-axle bogie and a model with two wheelsets. Along with this, in [12,20], special attention was paid to mathematical modeling of the dynamics of rotor systems, and in [13-19] – to the modeling of the dynamics of flexible rotors and a numerical method for solving the equation of motion of a rotor system with supports. A special elastic finite element was used to solve the problem [21].

It should also be noted that the determination of the dynamic characteristics of various structures [22-26], along with the rotating elements of machines, plays a certain role in predicting the dynamic behavior of these structures.

In the above studies, each approach and method has its own advantages and disadvantages. Despite this, they all are applied in solving various practical problems.

From the review of the above studies, one can notice the incompleteness of research, especially in the field of accounting for the gyroscopic effect and internal damping when determining the dynamic characteristics of rotating shafts with disks.

Therefore, this article is devoted to the development of mathematical models for assessing dynamic processes in deformable shafts with a rigid disk, taking into account the gyroscopic effect and internal damping, as well as determining their dynamic characteristics, which is a relevant problem at present.

2. Methods

Simulation of dynamic processes on a rotating shaft. An element (of the finite element model) is considered, isolated from a circular section shaft (Fig. 1) of length l with the beginning of the node A and the end B. The deformations of the element at any point x are described by deflections $u(x)$ (in the x direction), $v(x)$ (in the y direction), $w(x)$ (in the z direction), the Euler angles of rotation of the section plane $\vartheta(x)$, $\psi(x)$ and torsional rotation $\varphi(x)$. It is assumed that the section plane $\eta\zeta$ after straining remains perpendicular to the axis of the deformed shaft.

To obtain the corresponding finite element matrices, the kinetic and potential energies of the shaft element are used and then substituted into the Lagrange equation. In this case, to determine the kinetic energy, it is necessary to determine the velocity of the material point of the shaft element, located at a distance x from the origin.

When using the expansion of the basic motion at the point S (i.e., at the center of mass), of an element of length dx (Fig. 1), the speed of the sliding motion in the xyz coordinates is

$$\boldsymbol{v}(x) = \begin{bmatrix} \dot{u}(x) \\ \dot{v}(x) + w \cdot \omega_0 \\ \dot{w}(x) + v \cdot \omega_0 \end{bmatrix}. \quad (1)$$

The instantaneous angular velocity of the relative spherical motion about the XYZ coordinate system, taking into account the small strain angles $\vartheta(x)$ and $\psi(x)$, is described in the $\xi\eta\zeta$ coordinates, i.e.:

$$\boldsymbol{\omega}(x) = \begin{bmatrix} \omega_0 + \dot{\varphi} \\ -\omega_0\psi + \dot{\vartheta} \\ -\omega_0\vartheta + \dot{\psi} \end{bmatrix}. \quad (2)$$

The kinetic energy of the e-th finite element of the shaft is determined by the sum:

$$E_k^{(e)} = E_{k\,\mathrm{pos}}^{(e)} + E_{k\,\mathrm{sfer}}^{(e)}, \quad (3)$$

where $E_{k\,\mathrm{pos}}^{(e)}$ is the kinetic energy from the sliding motion, and $E_{k\,\mathrm{sfer}}^{(e)}$ is the kinetic energy from the spherical motion. These energies are determined by integration over the length of the element, i.e.:

$$E_{k\,\mathrm{pos}}^{(e)} = \frac{1}{2}\int_0^l A\,(x)\boldsymbol{v}(x)^T\boldsymbol{v}(x)\rho dx,\; E_{k\,\mathrm{sfer}}^{(e)} = \frac{1}{2}\int_0^l \boldsymbol{\omega}^T(x)\,\boldsymbol{J}(x)\boldsymbol{\omega}(x)\rho\mathrm{d}x, \tag{4}$$

where $A(x)$ is the cross-sectional area, ρ is the density of the material, and $\boldsymbol{J}(x) = diag\left(J_p(x), J(x), J(x)\right)$ is a diagonal matrix defined in terms of polar $J_p(x)$ and quadratic $J(x)$ moments of the shaft section. Substituting relations (1) - (2) into (4), we obtain:

$$E_{k\,\mathrm{pos}}^{(e)} = \frac{1}{2}\int_0^l A\,(x)\big[\dot{u}^2\,(x) + \dot{v}^2\,(x) + \dot{w}^2\,(x) - 2\,\dot{v}\,(x)\omega_0 w(x) + 2\,\dot{w}\,(x)\omega_0 v(x) + \\ + \big(w^2(x) + v^2(x)\big)\omega_0^2\big]\rho\mathrm{d}x,$$

$$E_{k\,\mathrm{sfer}}^{(e)} = \frac{1}{2}\int_0^l \Big[J_p(x)\left(\omega_0^2 + 2\omega_0\,\dot{\varphi}\,(x) + \dot{\varphi}^2\,(x)\right) + J(x)\left(\omega_0^2\psi^2(x) - 2\omega_0\psi(x)\,\dot{\vartheta}\,(x) + \\ + \dot{\vartheta}^2\,(x)\right) + J(x)\left(\omega_0^2\vartheta^2(x) + 2\omega_0\vartheta(x)\,\dot{\psi}\,(x) + \dot{\psi}^2\,(x)\right)\Big]\rho\mathrm{d}x. \tag{5}$$

The potential energy of the strained *e*-th finite element of the shaft is determined as:

$$E_p^{(e)} = \frac{1}{2}\int_0^l \int_{(A(x))} \Big[E\,\varepsilon_x^2(x) + G\left(\gamma_{xy}^2(x) + \gamma_{xz}^2(x)\right)\Big]\,dA(x)dx, \tag{6}$$

where E is the tensile modulus and G is the shear elastic modulus of the material.

Assuming the incompressibility of the cross-section of the shaft, we can determine the components of the displacement vector of an arbitrary point of the shaft relative to $\psi(x) = v'(x)$, $\vartheta(x) = -w'(x)$, i.e.:

$$\varepsilon_x = u'(x) - yv''(x) - zw''(x), \gamma_{xy} = -z\varphi'(x), \gamma_{xz} = y\varphi'(x). \tag{7}$$

Substitution of (7) into the expression for potential energy (6) results in:

$$E_p^{(e)} = \frac{1}{2}\int_0^l \int_{(A(x))} \Big[E\big(u'(x) - yv''(x) - zw''(x)\big)^2 + G\varphi'^2(x)(y^2 + z^2)\Big]\,\mathrm{d}A(x)\mathrm{d}x. \tag{8}$$

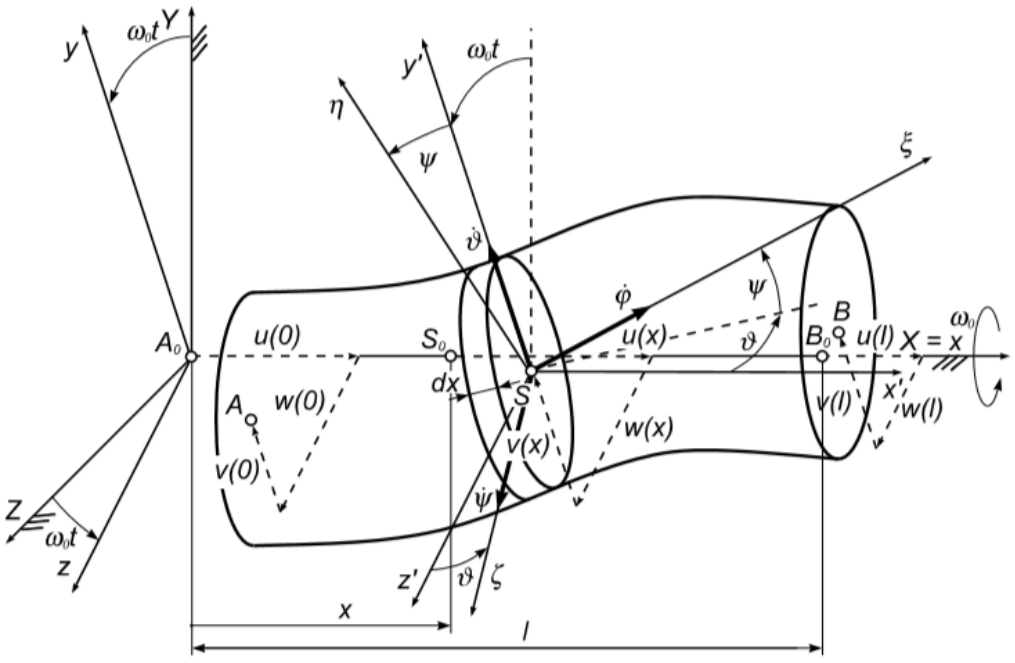

Fig.1. Scheme of the *e*-th finite element detailed from the circular section shaft

The components of the displacement vector inside the *e*-th finite element of the shaft are approximated by a linear and cubic function (a polynomial), i.e.:

$$v(x) = \boldsymbol{\Phi}(x)\boldsymbol{c}_1,\; \psi(x) = v'(x) = \boldsymbol{\Phi}'(x)\boldsymbol{c}_1, u(x) = \boldsymbol{\Psi}(x)\boldsymbol{c}_3,\; \varphi(x) = \boldsymbol{\Psi}(x)\boldsymbol{c}_4,$$
$$w(x) = \boldsymbol{\Phi}(x)\boldsymbol{c}_2,\; \vartheta(x) = -w'(x) = -\boldsymbol{\Phi}'(x)\boldsymbol{c}_2, \boldsymbol{\Phi}(x) = [1\; x\; x^2\; x^3], \boldsymbol{\Psi}(x) = [1\; x]. \tag{9}$$

To describe the strained state of the e-th finite element of the shaft in the xyz coordinate system, we use the vector of generalized displacements of the nodes A (for $x = 0$) and B (for $x = l$)

$$\tilde{\boldsymbol{q}}^{(e)} = [\boldsymbol{q}_1^T \boldsymbol{q}_2^T \boldsymbol{q}_3^T \boldsymbol{q}_4^T]^T, \tag{10}$$

where

$$\boldsymbol{q}_1 = \begin{bmatrix} v(0) \\ \psi(0) \\ v(x) \\ \psi(x) \end{bmatrix}, \ \boldsymbol{q}_2 = \begin{bmatrix} w(0) \\ \vartheta(0) \\ w(x) \\ \vartheta(x) \end{bmatrix}, \ \boldsymbol{q}_3 = \begin{bmatrix} u(0) \\ u(l) \end{bmatrix}, \ \boldsymbol{q}_4 = \begin{bmatrix} \varphi(0) \\ \varphi(l) \end{bmatrix}. \tag{11}$$

Using approximation relations (9) for the end nodes A and B of the shaft, we obtain

$$\boldsymbol{q}_i = \boldsymbol{S}_i \boldsymbol{c}_i, \ i = 1,2,3,4, \tag{12}$$

where $\boldsymbol{S}_1 = \begin{bmatrix} 1 & 0 & 0 & 0 \\ 0 & 1 & 0 & 0 \\ 1 & l & l^2 & l^3 \\ 0 & 1 & 2l & 3l^2 \end{bmatrix}, \ \boldsymbol{S}_2 = \begin{bmatrix} 1 & 0 & 0 & 0 \\ 0 & -1 & 0 & 0 \\ 1 & l & l^2 & l^3 \\ 0 & -1 & -2l & -3l^2 \end{bmatrix}, \ \boldsymbol{S}_3 = \begin{bmatrix} 1 & 0 \\ 1 & l \end{bmatrix}.$ (13)

Eliminating the unknown vectors $\boldsymbol{c}_i$ of the coefficient of approximating functions (12), we obtain approximation relations connecting the components of the displacement and strain vector through the generalized displacements of the nodes, i.e.:

$$\boldsymbol{u}(x) = \boldsymbol{\Psi}(x)\boldsymbol{S}_3^{-1}\boldsymbol{q}_3, \boldsymbol{v}(x) = \boldsymbol{\Phi}(x)\boldsymbol{S}_1^{-1}\boldsymbol{q}_1, \boldsymbol{w}(x) = \boldsymbol{\Phi}(x)\boldsymbol{S}_2^{-1}\boldsymbol{q}_2,$$
$$\boldsymbol{\psi}(x) = \boldsymbol{\Phi}'(x)\boldsymbol{S}_1^{-1}\boldsymbol{q}_1, \boldsymbol{\vartheta}(x) = -\boldsymbol{\Phi}'(x)\boldsymbol{S}_2^{-1}\boldsymbol{q}_2, \boldsymbol{\varphi}(x) = \boldsymbol{\Psi}(x)\boldsymbol{S}_3^{-1}\boldsymbol{q}_4. \tag{14}$$

The kinetic (5) and potential energy (8) of the e-th finite element of the shaft can be rewritten in matrix form using the approximation relations (14)

$$E_k^{(e)} = \frac{1}{2}\left(\dot{\tilde{\boldsymbol{q}}}^{(e)}\right)^T \tilde{\boldsymbol{M}}^{(e)}\dot{\tilde{\boldsymbol{q}}}^{(e)} + \omega_0\left(\dot{\tilde{\boldsymbol{q}}}^{(e)}\right)^T \tilde{\boldsymbol{C}}^{(e)}\tilde{\boldsymbol{q}}^{(e)} + \frac{1}{2}\omega_0^2\left(\tilde{\boldsymbol{q}}^{(e)}\right)^T \tilde{\boldsymbol{K}}_d^{(e)}\tilde{\boldsymbol{q}}^{(e)} +$$
$$+\omega_0\left(\dot{\tilde{\boldsymbol{q}}}^{(e)}\right)^T \tilde{\boldsymbol{f}}_1^{(e)} + \frac{1}{2}\omega_0^2 I^{(e)}, \quad E_p^{(e)} = \frac{1}{2}\left(\tilde{\boldsymbol{q}}^{(e)}\right)^T \tilde{\boldsymbol{K}}_s^{(e)}\tilde{\boldsymbol{q}}^{(e)}, \tag{15}$$

where $\tilde{\boldsymbol{M}}^{(e)}$ is the mass matrix, $\tilde{\boldsymbol{C}}^{(e)}$ is the Coriolis matrix, $\tilde{\boldsymbol{K}}_d^{(e)}$ is the reduced rotation matrix, $\tilde{\boldsymbol{f}}_1^{(e)}$ is the vector of gyroscopic forces, acting on the e-th finite element, $\tilde{\boldsymbol{K}}_s^{(e)}$ is the static stiffness matrix and $I^{(e)}$ is the moment of inertia of the e-th finite element of the shaft, which expresses the kinetic energy of a rotating unstrained element that rotates with a constant angular velocity ω_0.

The matrix and vector of the e-th finite element of the shaft have the following form:

$$\tilde{\boldsymbol{M}}^{(e)} = \begin{bmatrix} \boldsymbol{S}_1^{-T}(\boldsymbol{I}_1 + \boldsymbol{I}_2)\boldsymbol{S}_1^{-1} & \boldsymbol{0} & \boldsymbol{0} & \boldsymbol{0} \\ \boldsymbol{0} & \boldsymbol{S}_2^{-T}(\boldsymbol{I}_1 + \boldsymbol{I}_2)\boldsymbol{S}_2^{-1} & \boldsymbol{0} & \boldsymbol{0} \\ \boldsymbol{0} & \boldsymbol{0} & \boldsymbol{S}_3^{-T}\boldsymbol{I}_4\boldsymbol{S}_3^{-1} & \boldsymbol{0} \\ \boldsymbol{0} & \boldsymbol{0} & \boldsymbol{0} & \boldsymbol{S}_3^{-T}\boldsymbol{I}_5\boldsymbol{S}_3^{-1} \end{bmatrix}, \tag{16}$$

$$\tilde{\boldsymbol{C}}^{(e)} = \begin{bmatrix} \boldsymbol{0} & -\boldsymbol{S}_1^{-T}(\boldsymbol{I}_1 + \boldsymbol{I}_2)\boldsymbol{S}_2^{-1} & \boldsymbol{0} & \boldsymbol{0} \\ \boldsymbol{S}_2^{-T}(\boldsymbol{I}_1 + \boldsymbol{I}_2)\boldsymbol{S}_1^{-1} & \boldsymbol{0} & \boldsymbol{0} & \boldsymbol{0} \\ \boldsymbol{0} & \boldsymbol{0} & \boldsymbol{0} & \boldsymbol{0} \\ \boldsymbol{0} & \boldsymbol{0} & \boldsymbol{0} & \boldsymbol{0} \end{bmatrix}, \tag{17}$$

$$\tilde{\boldsymbol{K}}_d^{(e)} = \begin{bmatrix} \boldsymbol{S}_1^{-T}(\boldsymbol{I}_1 + \boldsymbol{I}_2)\boldsymbol{S}_2^{-1} & \boldsymbol{0} & \boldsymbol{0} & \boldsymbol{0} \\ \boldsymbol{0} & \boldsymbol{S}_2^{-T}(\boldsymbol{I}_1 + \boldsymbol{I}_2)\boldsymbol{S}_2^{-1} & \boldsymbol{0} & \boldsymbol{0} \\ \boldsymbol{0} & \boldsymbol{0} & \boldsymbol{0} & \boldsymbol{0} \\ \boldsymbol{0} & \boldsymbol{0} & \boldsymbol{0} & \boldsymbol{0} \end{bmatrix}, \tag{18}$$

$$\tilde{\boldsymbol{K}}_s^{(e)} = \begin{bmatrix} \boldsymbol{S}_1^{-T}\boldsymbol{I}_3\boldsymbol{S}_1^{-1} & \boldsymbol{0} & \boldsymbol{0} & \boldsymbol{0} \\ \boldsymbol{0} & \boldsymbol{S}_2^{-T}\boldsymbol{I}_3\boldsymbol{S}_2^{-1} & \boldsymbol{0} & \boldsymbol{0} \\ \boldsymbol{0} & \boldsymbol{0} & \boldsymbol{S}_3^{-T}\boldsymbol{I}_6\boldsymbol{S}_3^{-1} & \boldsymbol{0} \\ \boldsymbol{0} & \boldsymbol{0} & \boldsymbol{0} & \boldsymbol{S}_3^{-T}\boldsymbol{I}_7\boldsymbol{S}_3^{-1} \end{bmatrix}, \tag{19}$$

$$\tilde{\boldsymbol{f}}_1^{(e)} = [\mathbf{0} \quad \mathbf{0} \quad \mathbf{0}\, \boldsymbol{I}_8^T \boldsymbol{S}_3^{-1}]^T. \tag{20}$$

Here the quantities in (16) - (20) have the form:

$$\boldsymbol{I}_1 = \int_0^l \rho A(x)\, \boldsymbol{\Phi}^T(x)\boldsymbol{\Phi}(x)dx, \qquad \boldsymbol{I}_2 = \int_0^l \rho J(x)\, \boldsymbol{\Phi}'^T(x)\boldsymbol{\Phi}'(x)dx,$$

$$\boldsymbol{I}_3 = \int_0^l EJ(x)\, \boldsymbol{\Phi}''^T(x)\boldsymbol{\Phi}''(x)dx, \qquad \boldsymbol{I}_4 = \int_0^l \rho A(x)\, \boldsymbol{\Psi}^T(x)\boldsymbol{\Psi}(x)dx,$$

$$\boldsymbol{I}_5 = 2\int_0^l \rho J(x)\, \boldsymbol{\Psi}^T(x)\boldsymbol{\Psi}(x)dx, \qquad \boldsymbol{I}_6 = \int_0^l EA(x)\, \boldsymbol{\Psi}'^T(x)\boldsymbol{\Psi}'(x)dx,$$

$$\boldsymbol{I}_7 = 2\int_0^l GJ(x)\, \boldsymbol{\Psi}'^T(x)\boldsymbol{\Psi}'(x)dx, \qquad \boldsymbol{I}_8 = 2\int_0^l \rho J(x)\, \boldsymbol{\Psi}^T(x)dx\,. \tag{21}$$

The values that include the spherical motion of the shaft are represented by integral matrices $\boldsymbol{I}_2$ and $\boldsymbol{I}_5$.

In the case of a prismatic shaft ($A\,(x) = A,\ J(x) = J$), the integral matrices in (21) have the form

$$\boldsymbol{I}_1 = \varrho Al \begin{bmatrix} 1 & l/2 & l^2/3 & l^3/4 \\ l/2 & l^2/3 & l^3/4 & l^4/5 \\ l^2/3 & l^3/4 & l^4/5 & l^5/6 \\ l^3/4 & l^4/5 & l^5/6 & l^6/7 \end{bmatrix}, \qquad \boldsymbol{I}_2 = \varrho Jl \begin{bmatrix} 0 & 0 & 0 & 0 \\ 0 & 1 & l & l^2 \\ 0 & l & 4l^2/3 & 3l^3/2 \\ 0 & l^2 & 3l^3/2 & 9l^4/5 \end{bmatrix}$$

$$\boldsymbol{I}_3 = EJl \begin{bmatrix} 0 & 0 & 0 & 0 \\ 0 & 0 & 0 & 0 \\ 0 & 0 & 4 & 6l \\ 0 & 0 & 6l & 12l^2 \end{bmatrix}, \quad \boldsymbol{I}_4 = \varrho Al \begin{bmatrix} 1 & l/2 \\ l/2 & l^2/3 \end{bmatrix}, \quad \boldsymbol{I}_5 = \varrho J_p l \begin{bmatrix} 1 & l/2 \\ l/2 & l^2/3 \end{bmatrix},$$

$$\boldsymbol{I}_6 = EAl \begin{bmatrix} 0 & 0 \\ 0 & 1 \end{bmatrix}, \quad \boldsymbol{I}_7 = GJ_p l \begin{bmatrix} 0 & 0 \\ 0 & 1 \end{bmatrix}, \tag{22}$$

where $J_p = 2J$, ϱ is the density of the material, E and G are the constants of the elastic material (i.e., the moduli of elasticity under tension and shear).

After discretizing the one-dimensional continuum (a shaft) into finite elements and using the finite element method procedure and (15), with corresponding matrices, vectors for finite elements and the permutation matrix $\boldsymbol{P}\epsilon\boldsymbol{R}^{12,12}$ $\boldsymbol{X}^{(e)} = \boldsymbol{P}^T\widetilde{\boldsymbol{X}}^{(e)}\boldsymbol{P}$, $\boldsymbol{X} = \boldsymbol{M}, \boldsymbol{C}, \boldsymbol{K}_d, \boldsymbol{K}_s$, we obtain the following expression for the energy for the shaft (a continuum)

$$E_k = \sum_{e=1}^{N} E_k^{(e)} = \frac{1}{2}\boldsymbol{q}^T\boldsymbol{M}\dot{\boldsymbol{q}} + \omega_0(\dot{\boldsymbol{q}})^T\boldsymbol{C}\boldsymbol{q} + \frac{1}{2}\omega_0^2(\boldsymbol{q})^T\boldsymbol{K}_d\boldsymbol{q} + \omega_0(\dot{\boldsymbol{q}})^T\boldsymbol{f}_1 + \frac{1}{2}\omega_0^2 I,$$

$$E_p = \sum_{e=1}^{N} E_p^{(e)} = \frac{1}{2}(\boldsymbol{q})^T\boldsymbol{K}_s\boldsymbol{q}, \tag{23}$$

where N is the number of finite elements into which the considered shaft is partitioned, $\boldsymbol{M}$ is the global mass matrix, $\boldsymbol{C}$ is the global Coriolis matrix, $\boldsymbol{f}_1$ is the global vector of gyroscopic forces, $\boldsymbol{I}$ is the total moment of inertia of the shaft around the $\boldsymbol{x}$ axis, $\boldsymbol{K}_d$ is the global matrix of rotating reduction, $\boldsymbol{K}_s$ is the global static stiffness matrix, and $\boldsymbol{q}$ is the matrix of the global vector of node deviations (generalized coordinate vector), in the form

$$\boldsymbol{q} = [\boldsymbol{q}_i],\ \boldsymbol{q}_i = [u(x), v(x), w(x), \varphi(x), \vartheta(x), \psi(x)]^T,\ i = 1,2,\dots,N, N+1. \tag{24}$$

The Lagrange equations for the shaft (without damping and external excitation) in matrix form can be written as

$$\frac{d}{dt}\left(\frac{\partial E_k}{\partial \dot{\boldsymbol{q}}}\right) - \left(\frac{\partial E_k}{\partial \boldsymbol{q}}\right) + \left(\frac{\partial E_p}{\partial \boldsymbol{q}}\right) = 0. \tag{25}$$

Substituting the expression for the kinetic and potential energy (23) into the Lagrange equations (25), we obtain a system of ordinary differential equations in matrix form describing the motion of a rotating shaft taking into account the above factors, i.e.:

$$\boldsymbol{M}\ddot{\boldsymbol{q}}(t) + \omega_0\boldsymbol{G}\dot{\boldsymbol{q}}(t) + (\boldsymbol{K}_s - \omega_0^2\boldsymbol{K}_d)\boldsymbol{q}(t) = \boldsymbol{0}. \quad (26)$$

Here: $\omega_0\boldsymbol{G} = \omega_0(\boldsymbol{C} - \boldsymbol{C}^T)$ is the global matrix of gyroscopic effects.

Simulation of dynamic processes in the rigid disks. The rigid disk model can be used as a simplified model of gears, couplings, wheels of railway vehicles, etc.

Therefore, in this section, we will consider the constructed mathematical model for describing dynamic processes in the rigid disks in rotating coordinates. For this, a disk (Fig. 2) is considered with mass m as a rotating symmetric one and it has a center of mass at point S. Suppose that the origin of the Cartesian coordinate system $\xi\eta\zeta$ is at the center of mass of the disk, i.e. at point S and the coordinate system is rigidly connected to the disk. Then the distribution of the disk weight can be described by the inertia matrix $I_S = diag(I_0,\ I,\ I)$, in which these moments of inertia were determined around individual axes $I_0 = I_\xi,\ I = I_\eta = I_\zeta$ [4]. Further, considering the second Cartesian coordinate system xyz, which rotates around the x-axis with a constant angular velocity ω_0, which corresponds to the nominal angular velocity of the body ω. The oscillatory motion of the disk is described by displacements u, v, and w, respectively, in the directions of the x, y, and z axes and at the Euler angles of φ, ϑ, and ψ. The general spatial motion of the body is resolved into translational motion, described by a velocity vector with components in a rotating coordinate xyz as

$$\boldsymbol{v_S}(\boldsymbol{t}) = \begin{bmatrix} \dot{\boldsymbol{u}}(\boldsymbol{t}) \\ \dot{\boldsymbol{v}}(\boldsymbol{t}) - \boldsymbol{\omega_0 w}(\boldsymbol{t}) \\ \dot{\boldsymbol{w}}(\boldsymbol{t}) + \boldsymbol{\omega_0 v}(\boldsymbol{t}) \end{bmatrix}, \quad (27)$$

and the relative spherical motion around the center of mass of the disk S, which is determined in the coordinate system $\xi\eta\zeta$ by the angular velocity vector

$$\boldsymbol{\omega}(\boldsymbol{t}) = \begin{bmatrix} \boldsymbol{\omega_0}\,\boldsymbol{cos}(\boldsymbol{\vartheta}(\boldsymbol{t}))\,\boldsymbol{cos}(\boldsymbol{\psi}(\boldsymbol{t})) + \dot{\boldsymbol{\vartheta}}(\boldsymbol{t})\,\boldsymbol{sin}(\boldsymbol{\psi}(\boldsymbol{t})) + \dot{\boldsymbol{\varphi}}(\boldsymbol{t}) \\ \dot{\boldsymbol{\vartheta}}(\boldsymbol{t})\,\boldsymbol{cos}(\boldsymbol{\psi}(\boldsymbol{t})) - \boldsymbol{\omega_0}\,\boldsymbol{cos}(\boldsymbol{\vartheta}(\boldsymbol{t}))\boldsymbol{sin}(\boldsymbol{\psi}(\boldsymbol{t})) \\ \dot{\boldsymbol{\psi}}(\boldsymbol{t}) + \boldsymbol{\omega_0 sin}(\boldsymbol{\vartheta}(\boldsymbol{t})) \end{bmatrix}. \quad (28)$$

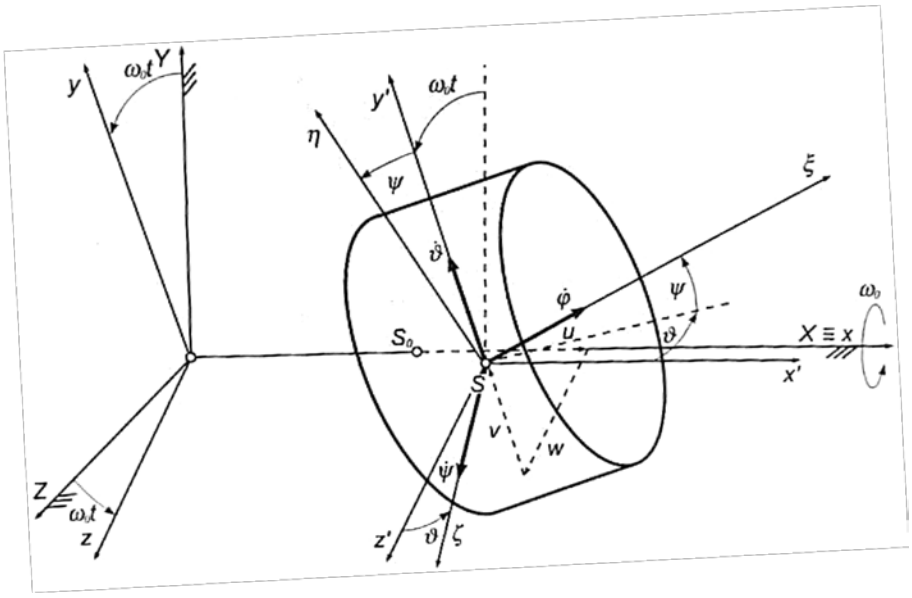

Fig. 2. Rigid disk in a rotating coordinate system

Taking into account the smallness of the angles of rotation ($\dot{\varphi}, \dot{\vartheta} \ll \omega_0$), expression (28) can be simplified, i.e.:

$$\boldsymbol{\omega}(\mathbf{t}) = \begin{bmatrix} \boldsymbol{\omega_0} + \dot{\boldsymbol{\vartheta}}(\mathbf{t})\boldsymbol{\psi}(\mathbf{t}) + \dot{\boldsymbol{\varphi}}(\mathbf{t}) \\ \dot{\boldsymbol{\vartheta}}(\mathbf{t}) - \boldsymbol{\omega_0}\boldsymbol{\psi}(\mathbf{t}) \\ \dot{\boldsymbol{\psi}}(\mathbf{t}) + \boldsymbol{\omega_0}\boldsymbol{\vartheta}(\mathbf{t}) \end{bmatrix}. \quad (29)$$

In this case, the kinetic energy of the disk is determined as follows:

$$E_k = \frac{1}{2} m\boldsymbol{v}_S^T\boldsymbol{v}_S + \frac{1}{2}\boldsymbol{\omega}^T\boldsymbol{I}_S\boldsymbol{\omega}. \quad (30)$$

After substituting (27) and (29) into (30) and after some correction, we get:

$$E_k = \frac{1}{2}m\dot{u}^2 + \frac{1}{2}m(\dot{v} - \omega_0 w)^2 + \frac{1}{2}m(\dot{w} + \omega_0 v)^2 + \frac{1}{2}[I_0(\omega_0 + \dot{\varphi})^2 + 2\omega_0\dot{\vartheta}\psi] + \\ + \frac{1}{2}I\left(\dot{\vartheta} - \omega_0\psi\right)^2 + \frac{1}{2}I(\dot{\psi} + \omega_0\vartheta)^2. \quad (31)$$

Substituting (31) into the Lagrange equation allows us to obtain a system of ordinary differential equations in matrix form which describes the motion of a rigid disk:

$$\frac{d}{dt}\left(\frac{\partial E_k}{\partial \dot{\boldsymbol{q}}_D}\right) - \left(\frac{\partial E_k}{\partial \boldsymbol{q}_D}\right) + \left(\frac{\partial E_p}{\partial \boldsymbol{q}}\right) = \boldsymbol{M}_D\ddot{\boldsymbol{q}}_D(t) + \omega_0\boldsymbol{G}_D\dot{\boldsymbol{q}}_D(t) + (\omega_0^2\boldsymbol{K}_D)\boldsymbol{q}_D(t). \quad (32)$$

Here: $\boldsymbol{q}_D(t) = [u, v, w, \varphi, \vartheta, \psi]^T$ is the vector of generalized coordinates of the rigid disk. At that, $\boldsymbol{M}_D$ are the rigid disk mass matrices, which have the form:

$$\boldsymbol{M}_D = diag\,(m, m, m, I_0, I, I), \quad (33)$$

and the gyroscopic effect matrices of the rigid disk are:

$$\boldsymbol{G}_D = \begin{bmatrix} 0 & 0 & 0 & 0 & 0 & 0 \\ 0 & 0 & -2m & 0 & 0 & 0 \\ 0 & 2m & 0 & 0 & 0 & 0 \\ 0 & 0 & 0 & 0 & 0 & 0 \\ 0 & 0 & 0 & 0 & 0 & I_0 - 2I \\ 0 & 0 & 0 & 0 & 2I - I_0 & 0 \end{bmatrix}. \quad (34)$$

The rigid disk reduced rotation matrix $\boldsymbol{K}_{D\omega}$ is diagonal and has the form:

$$\boldsymbol{K}_{D\omega} = diag(0, m, m, 0, I, I). \quad (35)$$

It should be noted that for axisymmetric bodies in the form of a thin disk, $I_0 = 2I$ holds; it means the relationship between I_0 – the moment of inertia about the axis of rotation and I – the moment of inertia of the cross-section of the disk. More information on modeling rigid and flexible disks in dynamic processes is described in detail in the monograph [4].

3. Results and discussion

In this study, the determination of the dynamic characteristics (i.e., eigenfrequencies, modes, and decrement of oscillations) of a specific system (an object) is performed using the Altair Hyperworks and MATLAB software packages.

The dynamic characteristics of the system are determined by solving the problem of natural vibrations for the system under consideration. Natural vibrations are the most ordered motions of the system, occurring in the absence of external influences; all points of the system oscillate according to the same real or complex harmonic law, with different amplitudes. In this case, the real part of the complex eigenfrequency means the frequency of oscillations of the system, and the imaginary part determines the velocity of oscillation damping and has the meaning of the damping coefficient.

Determining the dynamic characteristics of a system is an important part of any dynamic analysis and it allows evaluating the dynamic behavior of a system (an object). When studying the natural vibrations of the system (determining the dynamic characteristics), a homogeneous system of ordinary differential equations (26) or (32) is solved.

The described method was used to evaluate the eigenfrequencies and modes of vibration of a simple test steel shaft of wheelsets mounted on two bearings (radial-axial and radial ones).

The tested wheelsets consist of a hollow shaft and two disks (Fig. 3). Calculations were made for wheelsets with the following parameters - geometric dimensions: inner diameter of the shaft d_{shaft} = 0.026 m; outer diameters of the shaft $D_1 = 0{,}130\,m$, $D_2 = 0{,}165\ m$, $D_3 = 0.194\,m, D_4 = 0.1475$ m, $D_5 = 0.179\,m$; the length of the shaft l = 2.216 m; bearing stiffness $k_b = 6e + 12\ [N/m]$, $k_a = 2e + 12\ [N/m]$; the moment of inertia of the disks $I_{10} = I_{20} = 54.69\ kg \cdot m^2, I_1 = I_2 = 27.88\ kg \cdot m^2$; mass of disks $m_1 = m_2 = 364.57$ kg; material properties: modulus of elasticity E = 2.1e+11 Pa, G = 8.076e+10 Pa; Poisson's ratio v = 0.30; specific gravity of the material ρ = 7850 kg/m^3.

Determination of the dynamic characteristics of a rotating wheelset without damping. In the case of non-rotating wheelsets (for $\omega_0 = 0$ rad/s), taking into account the bearings, the system of equations of motion has the following form:

$$\left(\boldsymbol{M} + \boldsymbol{M}_1^{(D)} + \boldsymbol{M}_2^{(D)}\right)\ddot{\boldsymbol{q}}(t) + (\boldsymbol{K_s} + \boldsymbol{K_B})\boldsymbol{q}(t) = \boldsymbol{0}, \tag{36}$$

where $\boldsymbol{K_B}$ - is the bearing stiffness matrix, $\boldsymbol{M}_1^{(D)}, \boldsymbol{M}_2^{(D)}$ are the disk mass matrices.

The system of equations (36) for determining the generalized eigenvalue problem can be written in the form

$$\left[(\boldsymbol{K_s} + \boldsymbol{K_B}) - \lambda_v\left(\boldsymbol{M} + \boldsymbol{M}_1^{(D)} + \boldsymbol{M}_2^{(D)}\right)\right]\boldsymbol{q} = \boldsymbol{0}, \tag{37}$$

where λ_v – the roots of the characteristic equation are the eigenvalues equal to the square of the eigenfrequencies Ω_v^2.

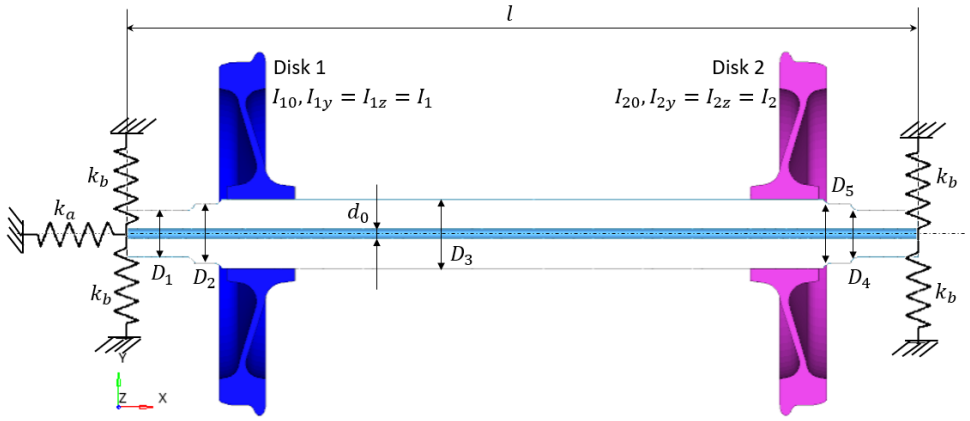

Fig. 3: Scheme of the tested wheelset

Table 1 shows the first eight eigenfrequencies $f_v = \Omega_v/2\pi$ of a non-rotating wheelset (as a deformable body) obtained using the Altair OptiStruct and MATLAB computer programs with short characteristics of the natural modes of vibration.

Table 1. Natural frequencies of the non-rotating wheelset

Number of eigenfrequencies f_v	Eigenfrequency f_v [Hz], MATLAB	Eigenfrequency f_v [Hz], Altair OptiStruct	Mode of vibration	Error [%]
1	0	0	Uniform rotation of the entire system (without twisting the shaft)	0
2.3	57.83	57.64	Bending mode of vibrations	0.34
4	80.07	86.26	Torsional mode of vibrations	7.17
5.6	163.6	170.11	Bending mode of vibrations	3.84
7.8	354.11	363.08	Bending mode of vibrations	2.46

Figure 4 shows some natural modes of vibration of wheelsets corresponding to multiple eigenfrequencies.

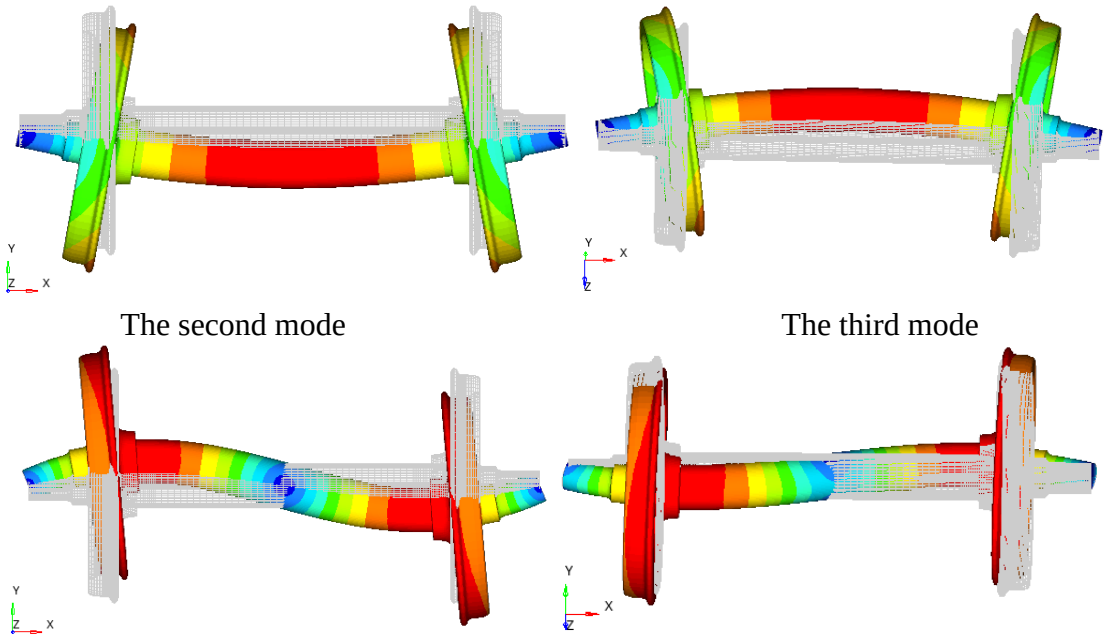

The second mode The third mode

The fifth mode The sixth mode

Fig. 4. Multiple natural modes of vibration of the non-rotating wheelset

Analysis of eigenfrequencies (Table 1) and modes of vibration (Fig. 4) shows that the first mode of vibration of rotating wheelsets is the motion of an absolutely rigid body with frequency $f_0 = 0$. An account for the elastic properties of the material of rotating shaft (as a deformable body) with two identical rigid disks leads to the appearance of multiple eigenfrequencies $f_{2,3}$ and $f_{5,6}$ with the corresponding modes of vibration.

In the case of a rotating shaft (at $\omega_0 \neq 0$ rad/s), the following aspects are taken into account: gyroscopic effects $(\omega_0(\boldsymbol{G}+\boldsymbol{G}_D)$ and the effect of rotation on the overall stiffness $(\omega_0^2(\boldsymbol{K}_d+\boldsymbol{K}_{D\omega})$.

The equation for determining the eigenvalues has the following form:

$$(\boldsymbol{K_s}+\boldsymbol{K_B}-\omega_0^2(\boldsymbol{K}_d+\boldsymbol{K}_{D\omega})\dot{\boldsymbol{q}}(t)-(\boldsymbol{K_s}+\boldsymbol{K_B}-\omega_0^2(\boldsymbol{K}_d+\boldsymbol{K}_{D\omega})\dot{\boldsymbol{q}}(t)=\boldsymbol{0}. \quad (38)$$

We transform the equation of motion (26) and (32) from the generalized coordinate space to the space $\boldsymbol{u}(\boldsymbol{t})=[\dot{\boldsymbol{q}}^{\boldsymbol{T}}(\boldsymbol{t}) \quad \boldsymbol{q}^{\boldsymbol{T}}(\boldsymbol{t})]^T$ of the state, that is, $\boldsymbol{u}(\boldsymbol{t}) \in \boldsymbol{R}^{\boldsymbol{2n}}$

$$\boldsymbol{S}\dot{\boldsymbol{u}}(t)+\boldsymbol{A}\boldsymbol{u}(\boldsymbol{t})=\boldsymbol{0}. \quad (39)$$

Here:

$$\boldsymbol{S}=\begin{bmatrix}(\boldsymbol{M}+\boldsymbol{M}_1^{(D)}+\boldsymbol{M}_2^{(D)}) & \boldsymbol{0}\\ \boldsymbol{0} & (\boldsymbol{K_s}+\boldsymbol{K_B}-\omega_0^2(\boldsymbol{K}_d+\boldsymbol{K}_{D\omega})\end{bmatrix} \text{ is an asymmetric matrix,} \quad (40)$$

$$\boldsymbol{A}=\begin{bmatrix}\omega_0(\boldsymbol{G}+\boldsymbol{G}_D) & (\boldsymbol{K_s}+\boldsymbol{K_B}-\omega_0^2(\boldsymbol{K}_d+\boldsymbol{K}_{D\omega})\\ -(\boldsymbol{K_s}+\boldsymbol{K_B}-\omega_0^2(\boldsymbol{K}_d+\boldsymbol{K}_{D\omega}) & \boldsymbol{0}\end{bmatrix} \text{ is an antisymmetric matrix.} \quad (41)$$

With (39) - (41) the eigenvalue problem is written in the form of a system of a homogeneous algebraic equation:

$$[\boldsymbol{A}-\lambda_v\boldsymbol{S}]\boldsymbol{u}=\boldsymbol{0}. \quad (42)$$

A nontrivial solution to system (42) is λ_v, that is, the eigenvalues of the characteristic determinant of equations (42), which are the imaginary value obtained due to the antisymmetry of the matrix $\omega_0(\boldsymbol{G}+\boldsymbol{G}_D)$.

The eigenvalues λ_ν of system (42) are a complex quantity, i.e. $\lambda_\nu = \pm i\Omega_\nu$, $\nu = 1, 2, \ldots, n$ and their imaginary part is the eigenfrequencies Ω_ν in rad/s of rotating wheelsets.

Figure 5 shows (full line) the dependence of the first eight eigenfrequencies $f_\nu = 2\pi\Omega_\nu$ (Hz) on the rotating speed of the wheelsets per minute (the so-called Campbell diagram) plotted in the angular velocity range from $\omega_0 = 0$ to $\omega_0 = 3500$ rpm.

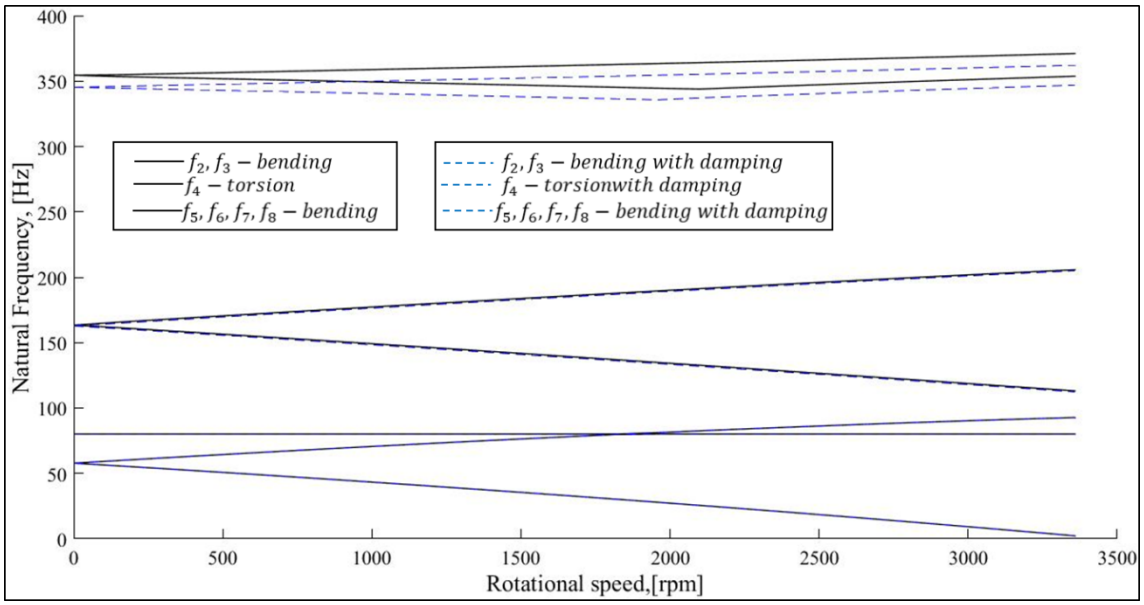

Fig. 5. Campbell diagram for rotating wheelset

Paired eigenfrequencies are divided into two branches, where the first increases and the second decreases depending on the angular velocity. This phenomenon is caused by gyroscopic effects. Obviously, the non-paired eigenfrequencies (f_4) do not depend on the rotating speed since this mode of vibrations does not affect the gyroscopic effects (torsional mode of vibrations).

Determination of dynamic characteristics of a rotating wheelset with damping. Rotating wheelsets are considered with an account for the damping properties of the shaft material. Generally, in the calculations, when solving practical problems in engineering, the damping matrix [12] is used, instead of viscous damping, in the form of a linear combination of the mass and stiffness matrices $\boldsymbol{B}_s = a\boldsymbol{M}_s + b\boldsymbol{K}_s$, a is the mass proportionality coefficient and b is the stiffness proportionality coefficient. The use of the damping matrix $\boldsymbol{B}_s = a\boldsymbol{M}_s + b\boldsymbol{K}_s$ simplifies the solution of practical problems.

When describing dynamic processes on a rotating shaft with rigid disks (wheelsets), with the damping coefficient, equation (42) ($\omega_0(\boldsymbol{G} + \boldsymbol{G}_D)$ is written using the damping matrix($\boldsymbol{B}_s$), in the form ($\omega_0(\boldsymbol{G} + \boldsymbol{G}_D) + \boldsymbol{B}_s$).

Specific calculations for the geometrical and physical-mechanical parameters of the rotating shaft and rigid disk (wheelsets) similar to the given above were obtained. The relative damping coefficients were determined from [12] using α_ν and β_ν, for $\omega_0 = 700$ rad/s and $a = 0, b = 0.0002$.

Further, using the developed model, the eigenfrequencies and the damping coefficient for rotating wheelsets were determined, taking into account the damping properties of the shaft material (Table 2). The damping coefficient D_ν was determined by the formula

$$D_\nu = \frac{-\alpha_\nu}{\sqrt{\alpha_\nu^2 + \beta_\nu^2}}. \quad (43)$$

Eigenfrequencies of the rotating wheelsets, considering damping, are given in Table 2.

Table 2. Natural frequencies of rotating wheelsets

Number of eigenfrequencies ν	Eigenfrequency f_ν (Hz), not considering damping (for $\omega_0 = 700$ rad/s)	Damping coefficients D_ν,	Eigenfrequency f_ν(Hz), considering damping (for $\omega_0 = 700$ rad/s) $\lambda_\nu = \alpha_\nu \pm i\,\beta_\nu$	Damping coefficients D_ν,
1	$-3.84e-6 \pm i\,0$	1	$0,0027 \pm i\,0$	1
2	$-1.72e-5 \pm i47.88$	3.59e-07	$-1.75 \pm i47.84$	0.0366
3	$-1.06e-05 \pm i66.97$	1.58e-07	$-2.45 \pm i66.93$	0.0366
4	$-2.02e-07 \pm i80.11$	2.52e-09	$-4.03 \pm i79.97$	0.0503
5	$-1.2e-03 \pm i153.60$	7.84e-06	$-15.80 \pm i152.73$	0.1029
6	$-1.6e-03 \pm i173.24$	9.28E-06	$-17.83 \pm i172.36$	0.1029
7	$-5.21e-05 \pm i350.8$	1.49e-07	$-78.06 \pm i341.96$	0.2225
8	$-5.27e-05 \pm i357.4$	1.48e-07	$-79.54 \pm i348.51$	0.2225

Table 2 shows the first eight eigenfrequencies of a rotating shaft (as a deformable body) with wheelsets (at ω_0 = 700 rad/s) with and without damping, obtained using the MATLAB software. The results obtained show that an account for the damping affects only the seventh and eighth eigenfrequencies. Figure 5 shows (dashed line) the dependence of the first eight eigenfrequencies on the damping. The remaining (the first six) eigenfrequencies are practically not affected by damping.

4. Conclusions

1. Mathematical models and methods for determining the dynamic characteristics (eigenfrequencies, modes, and decrement of oscillations) of railway wheelsets, taking into account internal damping and gyroscopic effect were developed in this study.
2. The eigenfrequencies, modes, and damping coefficient of rotating wheelsets at their different revolutions with and without damping were investigated.
3. As a result of studying the dynamic characteristics of rotating wheelsets, it was determined that:

– the values of the paired eigenfrequencies (f_2, f_3, f_5, f_6 and f_7, f_8) were divided into two groups; in the first group the values of (f_2, f_5, and f_7) increased, and in the second group the values of (f_3, f_6 and f_8) decreased depending on the angular velocity due to the influence of the gyroscopic effect;

– non-multiple eigenfrequencies (i.e.,$-$ f_4) did not depend on the rotation velocity since the gyroscopic effects did not affect the torsional modes;

– the damping effect did not affect the first 5 eigenfrequencies (f_2, f_3, f_4, f_5 and f_6), and when damping was taken into account, the seventh and eighth frequencies f_7, f_8 decreased insignificantly.

References

[1] Krämer E. *Dynamics of Rotors and Foundations*. Berlin: Springer; 2012.
[2] Wittenburg J. *Dynamics of Multibody Systems.* 2nd ed. Wittenburg; 2008.
[3] Yamamoto T. *Linear and Nonlinear Rotordynamics: A Modern Treatment with Applications*. New York: Wiley Interscience; 2012.
[4] Eliseev V. *Mechanics of a deformable rigid body*. Publishing House of the Polytechnic University; 2006.
[5] Kaiyun W, Chao H, Wanming Z, Pengfei L, Shen W. Progress on wheel-rail dynamic performance of railway curve negotiation. *Journal of Traffic and Transportation Engineering*. 2014;1(3): 209-220.

[6] Trimpe F, Lück S, Naumann R, Salander C. Simulation of Torsional Vibration of Driven Railway Wheelsets Respecting the Drive Control Response on the Vibration Excitation in the Wheel-Rail Contact. *Vibration*. 2021;4(1): 30-48.
[7] Xiaoqi M, Lin J, Liangliang H. A computational simulation study on the dynamic response of high-speed wheel–rail system in rolling contact. *Advances in Mechanical Engineering*. 2018;10(11): 1-11.
[8] Mikheev G, Pogorelov D, Rodkov A. Methods of Simulation of Railway Wheelset Dynamics taking into account Elasticity. In: *Proc. First International Conference on Rail Transportation*. China; 2017. DOI: 10.13140/RG.2.2.32562.25281.
[9] Vila P, Rovira A, Fayos J, Baeza L. Dynamic model of a railway wheelset for corrugation problem analysis. *Journal Noise and Vibration Worldwide*. 2009;40(11): 10-17.
[10] Torstensson PT, Nielsen JCO, Baeza L. Dynamic train-track interaction at high vehicle speeds-Modelling of wheelset dynamics and wheel rotation. *Journal of Sound and Vibration*. 2011;330(22): 5309-5321.
[11] Uyulan C, Gokasan M, Bogosyan S. Dynamic Investigation of the Hunting Motion of a Railway Bogie in a Curved Track via Bifurcation Analysis. *Mathematical Problems in Engineering*. 2017: 8276245.
[12] Byrtus M, Hajžman M, Zeman V. *Dynamika rotujících soustav*. ZČU v Plzni; 2010. (In Czech)
[13] Bykov V, Melnikov A. Mathematical model of a flexible rotor based on generalized Lagrangian coordinates. *Bulletin of St. Petersburg University*. 2010;4: 110-118.
[14] Tian Y, Zhaoab Y, Maa H, Yuan Z. Free vibration analysis of a rotating graphene nanoplatelet reinforced pre-twist blade-disk assembly with a setting angle. *Applied Mathematical Modelling*. 2021;93: 578-596.
[15] Eliseev V, Zinovieva T, Abid S. On the theory and methods of calculating the critical regimes of elastic rotor rotation. *Russian Internet Journal of Industrial Engineering*. 2017;5(3): 9-14.
[16] Polushkin O. Systematic laws of mechanics and balancing of rotors. *Bulletin of the Don State Technical University*. 2011;11(57): 842-849.
[17] Hui M, Qianbin Z, Xueyan Z, Qingkai H, Bangchun W. Dynamic characteristics analysis of a rotor–stator system under different rubbing forms. *Applied Mathematical Modelling, Elsevier*. 2015;39(8): 2392-2408.
[18] Solomin OV. Numerical methods for solving the equations of motion in problems of the dynamics of rotor systems with fluid friction supports. *Mechanical Engineering Magazine*. 2006;11: 16-26.
[19] Sperling L, Ryzhik B, Linz C, Duckstein H. Simulation of two-plane automatic balancing of a rigid rotor. *Mathematics and Computers in Simulation*. 2002;58: 351-365.
[20] Sašek JV. Eigenfrequency sensitivity analysis of flexible rotors. *Applied and Computational Mechanics*. 2007;1: 289-298.
[21] Kang Y, Chang Y, Tsai J, Mu L, Chang Y. An investigation in stiffness effects on dynamics of rotor-bearing-foundation systems. *Journal of Sound and Vibration*. 2000;231(2): 343-374.
[22] Mirsaidov M, Toshmatov E. Spatial stress state and dynamic characteristics of earth dams. *Magazine of Civil Engineering*. 2019;89(5): 3-15.
[23] Mirsaidov M, Troyanovsky I. Forced axisymmetric oscillations of a viscoelastic cylindrical shell. *Polymer Mechanics*. 1975;11(6): 953-955.
[24] Mirsaidov M, Mekhmonov Y. Nonaxisymmetric vibrations of axisymmetric structures with associated masses and hollows (protrusions). *Strength of Materials*. 1987;19(3): 424-430.

[25] Mirsaidov M, Abdikarimov R, Khudainazarov S, Sabirjanov T. Damping of high-rise structure vibrations with viscoelastic dynamic dampers. *E3S Web of Conferences*. 2020;224(02020): 1-14.
[26] Mirsaidov M, Dusmatov O, Khodjabekov M. The problem of mathematical modeling of a vibration protected rod under kinematic excitations. *IOP Conference Series: Materials Science and Engineering*. 2021;1030(1): 1-14.

THE AUTHORS

Ahmedov Olimjon
e-mail: olimjon84@mail.ru
ORCID: 0000-0002-1087-7303

Mirsaidov Mirziyod
e-mail: mirsaidov1948@mail.ru
ORCID: 0000-0002-8907-7869